THE ASTROPHYSICAL JOURNAL, 437:458–464, 1994 December 10

X-RAY EMISSION FROM PSR 0355+54

PATRICK SLANE
Harvard-Smithsonian Center for Astrophysics, 60 Garden Street, Cambridge, MA 02138; e-mail: slane@cfa.harvard.edu
Received 1994 April 7; accepted 1994 June 13

ABSTRACT

We have obtained a 20 ks observation of PSR 0355+54 using the *ROSAT* PSPC. The pulsar is detected with a count rate of $4.2(\pm 1.3) \times 10^{-3}$ s^{-1} above the background. While the $\sim$70 source counts are insufficient for spectral fitting, we have derived source parameters for specific cases of power law as well as blackbody spectra. For a Crab-like spectrum (photon index $\alpha = 2$) we find $L_x(0.1\text{–}2.4 \text{ keV}) = 1.0 \times 10^{32}$ ergs s^{-1}, somewhat higher than upper limits reported from *Einstein* observations but consistent with typical L_x versus $\dot{E}$ values for other pulsars. For blackbody emission, we derive a temperature upper limit of $\sim 9.5 \times 10^5$ K for emission from the entire neutron star surface, which is consistent with standard models for cooling of the neutron star interior given a characteristic age $10^{5.75}$ yr. No evidence is present for modulation at the 156 ms pulsar period, setting a weak upper limit of $\sim$75% for the pulsed fraction of the X-ray signal.

Subject headings: pulsars: individual (PSR 0355+54) — radiation mechanisms: nonthermal — X-rays: stars

1. INTRODUCTION

X-ray emission from isolated pulsars can originate from a number of distinct mechanisms. These can be categorized in terms of the energy source: cooling of the hot stellar interior; energy derived from the pulsar spin-down; or gravitational energy released upon accretion of material from the interstellar medium (ISM). The exact mechanism by which energy is produced in the X-ray band differs with each such scenario and may actually consist of several modes and/or production sites. Cooling, for example, manifests itself as blackbody emission from the entire surface of the neutron star (NS). However, the spectrum may be modified by the presence of a thin atmosphere, and the details of the atmospheric effects depend upon the surface magnetic field strength. Further, thermal conductivity gradients across the surface, produced by the star's magnetic field, may result in a nonuniform surface temperature. Spin-down energy, associated with acceleration of charged particles in the pulsar magnetosphere, may take the form of thermal emission from the heated polar caps, synchrotron radiation produced near the pulsar light cylinder, or a synchrotron nebula supported by the ambient medium and magnetic field. Accretion luminosity may be thermal or nonthermal depending upon the exact mechanism by which the matter reaches the NS surface. Studies of the X-ray emission from isolated pulsars may thus provide information about the interior stellar structure, the surface characteristics of the NS, and the geometry and dynamics of the pulsar magnetosphere and its surroundings. The reader is referred to recent reviews by Ögelman (1994) and Finley (1994) for summaries of the current status of such X-ray studies. Here we study emission from PSR 0355+54 to investigate specific emission scenarios and to compare results with those obtained for other pulsars.

PSR 0355+54 is a moderate-age, isolated pulsar (characteristic age $P/2\dot{P} = 10^{5.75}$ yr) with a fairly short period (156 ms). Radio studies show the pulsar to have relatively low timing noise, though occasional glitches have been observed including a massive glitch ($\Delta P/P = -4.4 \times 10^{-6}$) in 1986 (Lyne 1987) which was accompanied by a large change in spin-down rate. The postglitch relaxation was studied by Alpar, Pines, & Cheng (1988) in the context of a vortex creep model which describes the dynamical coupling of superfluid regions in the NS interior to the crust rotation. The primary properties as determined by radio observations (Taylor, Manchester, & Lyne 1993) are summarized in Table 1 where we have also listed properties for the similar pulsar PSR 1055−52.

Using the spin-down energy loss rate, $\dot{E}$, as an indicator, PSR 0355+54 is a good candidate for observable X-ray emission; only 10 of the 119 radio pulsars with distances, D, closer than PSR 0355+54 have larger values of $\dot{E}/D^2$, and eight of these are known X-ray emitters. X-ray observations of PSR 0355+54 were carried out with the *Einstein Observatory*, in a 19 ks pointing with the Imaging Proportional Counter (IPC), but the results were inconclusive. Weak emission from a position $\sim$1.7 from the radio position was detected, and Helfand (1983) suggested this could be evidence for extended emission from a synchrotron nebula associated with the pulsar. Seward & Wang (1988) considered the association tentative, reporting only an upper limit of $L_x < 4.8 \times 10^{31}$ ergs s^{-1}.

The study of this pulsar is particularly interesting because its properties are very similar to those of PSR 1055−52 (see Table 1), a known X-ray source (Cheng & Helfand 1983; Brinkmann & Ögelman 1987; Ögelman & Finley 1993) which has recently been detected as a γ-ray source as well (Fierro et al. 1993). The properties of PSR 0355+54 suggest a Vela-like pulsar very near the outer-gap death line for sustained γ-ray production (Chen & Ruderman 1993—see § 4), although it must be noted that this interpretation is somewhat dependent upon the inclination of the magnetic field relative to the pulsar spin axis; PSR 1055−52 has a radio pulse-interpulse separation of $\sim$180° (McCulloch et al. 1978), suggesting a large inclination angle, while the PSR 0355+54 radio profile shows a single peak (Morris et al. 1981) suggestive of a smaller inclination angle.

2. OBSERVATIONS

PSR 0355+54 was observed for 19,144 s, beginning on 1993 March 13, using the *ROSAT* Position Sensitive Proportional Counter (PSPC). The PSPC (Pfeffermann et al. 1986) provides coarse energy resolution ($\Delta E/E = 0.43[E/0.93]^{-0.5}$ [FWHM]) over the bandpass 0.1–2.4 keV along with position resolution of $\sim$25″ (FWHM). Event times are recorded with relative accuracies of $\sim$100 μs, but absolute time uncertainties as large

TABLE 1

PULSAR PARAMETERS FOR PSR 0355+54 AND PSR 1055−52

PSR	P (ms)	$\dot{P}/10^{-15}$ (s s^{-1})	log $\dot{E}$ (ergs s^{-1})	log T (yr)	DM (cm^{-3} pc)	D (kpc)	log B (G)
0355+54.....	156	4.4	34.66	5.75	57	2.07	11.92
1055−52.....	197	5.8	34.48	5.73	30	1.53	12.04

as 2 ms may occur over long periods (several days) due to clock drifts or resets. The PSR 0355+54 observation was carried out in 16 small segments spread over a ~3 day period. After cleaning the data by removing any time intervals at the ends of these segments which showed evidence of increases in count rate due to bright Earth effects, 16,644 s of good data remained. A faint X-ray source was detected at a nominal position R.A.(J2000) = 03^{h}58^{m}53^s.2, Decl.(J2000) = +54°13′00″.6, in good agreement with the pulsar position R.A.(J2000) = 03^{h}58^{m}53^s.7, Decl.(J2000) = +54°13′13″.58 (Taylor et al. 1993—see Fig. 1). The position discrepancy (13″.7) is within the expected deviations based upon the spatial response of the detector and the limited number of counts in the image. The pulsar count rate was determined by extracting counts inside a circle of radius 2′.5 centered on the source, using an annular region extending from 2′.5 to 8′.3 for background determination. We find $N = 70.6 \pm 21.7$ source counts, corresponding to a count rate of $R_{\rm PSPC} = 4.2(\pm 1.3) \times 10^{-3}$ s^{-1}. Data were restricted to PI bins 11–235 (PROS channels 3–33), corresponding to an energy band ~0.1–2.4 keV.

To search for evidence of extended emission we have smoothed the X-ray image with a 32″ Gaussian profile, and subtracted an identically selected and smoothed image of the calibration point source 3C 273 normalized to the same number of (background-subtracted) counts. The resulting profile indicates faint emission concentrated ~1′.6 from the pulsar, at a position angle approximately 72° north of east. This is consistent with the size of the offset described by Seward & Wang (1988) although the relative brightness of this region of enhancement is more than a factor of 5 smaller than that corresponding to the pulsar. The measured proper motion for PSR 0355+54 is $\mu_\alpha = 5 \pm 4$ mas yr^{-1}, $\mu_\delta = 6 \pm 3$ mas yr^{-1} (Lyne, Anderson, & Salter 1982). The sky projection of this motion corresponds, within uncertainties, to the direction to the enhanced emission. This may indicate that the emission, which appears ahead of the pulsar motion, is the result of synchrotron radiation from a wind-driven nebula supported by the ram pressure created by the proper motion through the ISM (Cheng 1983; Wang, Li, & Begelman 1993). However, based upon the space density of sources with similar brightness observed in the field, we do not consider the association between the pulsar and the faint residual source particularly compelling.

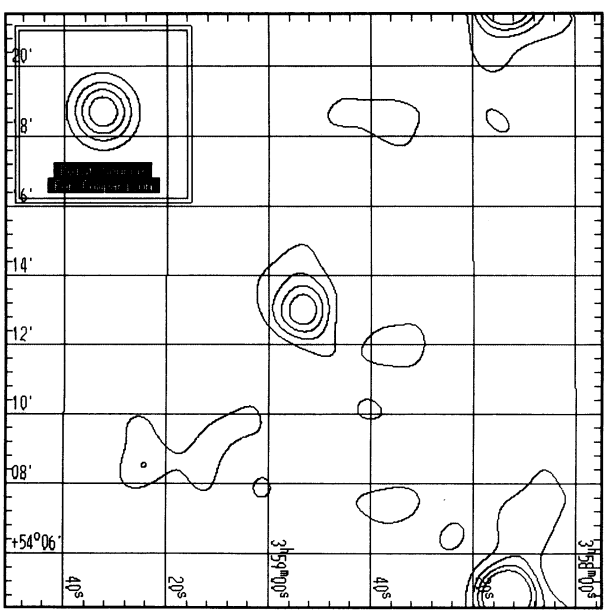

FIG. 1.—Contour plot of the X-ray emission from PSR 0355+54 (center). Contours are spaced at intervals of 20% of the pulsar peak emission. Inset image shows point source data from 3C 273, scaled to PSR 0355+54 flux levels. Images have been background-subtracted and smoothed with a 32″ Gaussian profile.

3. TIMING STUDIES

Using events extracted from a 30″ (radius) circle centered on the source, we have searched for evidence of pulsations at the known radio period of 156 ms. While excluding ~20%–30% of the source counts due to the finite spatial resolution of the mirror/PSPC system (the 90% fractional encircled energy radius ranges from ~35″ at 0.3 keV to ~50″ at 1.7 keV), this smaller source region reduces the background by a factor of greater than 30 over that in the 2′.5 circle used for determining the source strength, providing increased sensitivity for the detection of pulsations. Event times were propagated to the solar system barycenter using the radio pulsar coordinates, and the Z_n^2 test (Buccheri et al. 1983) was used to search for modulation at the fundamental and first harmonic frequencies:

$$Z_n^2 = \frac{2}{N} \sum_{k=1}^{n} \left[\left(\sum_{j=1}^{N} \cos k\phi_j \right)^2 + \left(\sum_{j=1}^{N} \sin k\phi_j \right)^2 \right], \quad (1)$$

where N is the total number of counts, ϕ_j is the phase associated with event time t_j (relative to the period being tested), and n is the number of harmonics being considered. A recent radio ephemeris (Table 2) spanning the observation interval was obtained from the pulsar data base maintained by the pulsar group at Princeton (as described by Taylor et al. 1993). We find no evidence for pulsations at the expected frequency, although the limited number of counts ($N = 61$) does not provide a high detection sensitivity. An upper limit to the pulsed power can be established based upon the Z_n^2 statistic (van der Klis 1989). For

TABLE 2

PSR 0355+54 PULSE EPHEMERIS

Parameter	Value
P(s)	0.15638220635
$\dot{P}$(s s^{-1})	4.39659×10^{-13}
T(JD)	2,449,060.0

the first harmonic, the pulsed power is

$$f = 2\sqrt{\frac{(Z_1^2/2) - 1}{N}} . \quad (2)$$

Since, for random event times, Z_1^2 is distributed as χ^2 for two degrees of freedom, the null detection permits us to establish a 3 σ upper limit $f \lesssim 50\%$. The expected number of background counts in the 30″ circle is ~ 16. Thus, the pulsed power from the pulsar alone is $\lesssim 77\%$. This value is clearly not very constraining; with the exception of the Crab pulsar, which is nearly 100% pulsed, most pulsars have pulsed components smaller than the upper limit derived for PSR 0355+54. Similar analysis for X-rays from PSR 1055−52, for example, reveals a broadband pulsed component of $\sim 8\%$. This component increases to $\sim 85\%$ when only higher energy ($E \gtrsim 0.5$ keV) photons are considered (see Ögelman & Finley 1993), but a corresponding effect in PSR 0355+54 would not be seen due to lack of photons.

4. SPECTRAL STUDIES

The PSR 0355+54 spectrum was extracted from a circular region of radius 2.5, with background determined from the surrounding annulus extending to 4.2. The limited number of photons precludes attempts at spectral fitting to characterize the X-ray emission. However, by considering the number of counts in broad energy bands, it is possible to calculate hardness ratios which provide considerable information about the spectrum. We have used the binning scheme adopted in the IRAF/PROS analysis software and have tabulated counts in the following bands (corresponding to those used in the PSPC standard processing): *A* ($11 \le$ PI ≤ 41), *B* ($52 \le$ PI ≤ 201), *C* ($52 \le$ PI ≤ 90), and *D* ($91 \le$ PI ≤ 201); corresponding PROS bin boundaries are 3–10 (*A*), 13–30 (*B*), 13–18 (*C*), and 19–30 (*D*). We then calculated the hardness ratios

$$H_1 = \frac{(B-A)}{(B+A)} = 0.51 \pm 0.40 ,$$
$$H_2 = \frac{(D-C)}{(D+C)} = 0.74 \pm 0.30 . \quad (3)$$

Using the same event selection criterion, we have calculated the hardness ratios for PSR 1055−52: $H_1 = -0.81 \pm 0.01$, $H_2 = -0.58 \pm 0.05$. Clearly the values for PSR 0355+54 suggest a spectrum which is either inherently harder than that of PSR 1055−52, or which is more strongly absorbed.

We have carried out a spectral fit for PSR 1055−52 using data from both the *ROSAT* PSPC and the *Einstein* IPC. We find the best fit for a two-component model (blackbody plus power law) with the parameters listed in Table 3; the temperature and power-law index are in good agreement with those determined by Ögelman & Finley (1993) using only PSPC data plus the additional constraint that the power-law index conform within 2 σ to that derived from the *Compton Gamma-Ray Observatory* (*CGRO*) data; our determination of the relative contribution between the two components differs somewhat, however. Using the best-fit value for N_H, we have estimated the column density for PSR 0355+54 by scaling this to the ratio of dispersion measures ($N_H = 6.1 \times 10^{20}$ cm^{-2}). We then folded the PSR 1055−52 model spectrum through the additional absorption to determine whether the difference in hardness ratios was an artifact of the column density. The hardness ratios for PSR 0355+54 are not reproduced by this process; the model spectrum is still considerably softer than that observed. However, the ISM ionization fraction toward PSR 1055−52 is likely to be much higher than that toward PSR 0355+54; with a dispersion measure of 30 cm^{-3} pc (Taylor et al. 1993), the N_H value for PSR 1055−52 derived from the X-ray data yields an ionization fraction of 0.22 which is in the upper range of expected values.

TABLE 3

PSR 1055−52 FIT: BLACKBODY + POWER LAW

Component	Parameter[a]	Value[b]
Blackbody	kT (keV)	61.8 ± 4.2
	F_x (ergs cm^{-2} s^{-1})	2.3×10^{-12}
Power law	α	1.5 ± 0.7
	$F_{x,}$ (ergs cm^{-2} s^{-1})	2.3×10^{-13}

[a] Flux evaluated in 0.1–2.4 keV energy band.

[b] For comparison, Ögelman & Finley 1993 find $F_{BB} = 1.1 \times 10^{-11}$ and $F_{PL} = 4.8 \times 10^{-14}$.

The value of N_H for PSR 0355+54 has been measured directly from 21 cm absorption observations (Gómez-Gonzàlez & Guélin 1974). Absorption features are observed over a velocity range ~ 0 to -25 km s^{-1} with optical depths $\tau < 0.15$ for an integrated total absorption $\int \tau\, dv = 11$ km s^{-1}. Assuming a hydrogen spin temperature $T_s = 100$ K, this yields $N_H = 2 \times 10^{21}$ cm^{-2}. Adopting this value with the spectral model for PSR 1055−52 yields hardness ratios closer to that observed for PSR 0355+54, though still somewhat softer than the observed values. Gómez-González & Guélin (1974) note that the 21 cm measurement for PSR 0355+54 was carried out at low resolution, so that the quoted total absorption is actually an underestimate. Increasing the N_H value somewhat over that derived above brings the model hardness ratios more into line with those observed, but still predicts a spectrum softer than that observed, possibly suggesting a weaker low-temperature thermal component than that of PSR 1055−52.

With the limited spectral information available, we can still consider two important scenarios for the emission from PSR 0355+54 which will help characterize the emission. We first consider the possibility that the X-ray flux is associated with thermal emission from the entire NS surface, as might be expected from cooling of the interior. We will show that this does not seem likely based upon the available data. Then we will derive the X-ray luminosity assuming Crab-like parameters for the emission, and investigate the associated X-ray luminosity in terms of the available spin-down power.

4.1. *Blackbody Emission*

After core collapse in a Type II supernova, a NS forms with an interior temperature of $\sim 10^{11}$–10^{12} K. Initial cooling proceeds rapidly through neutrino emission from the core, primarily generated through the direct Urca reactions. Subsequent cooling depends sensitively on the core equation of state as well as on the structure of the NS crust where neutrino bremsstrahlung may be important. As energy diffuses to the NS surface, it is radiated as blackbody emission with a characteristic temperature of 10^5–10^6 K, peaking in the soft X-ray band. X-ray studies thus provide the most sensitive probe of NS cooling and the star's internal structure, including (1) the possibility that the direct Urca process operates at lower temperatures (and, thus, later times) due to large central densities (Lattimer et al. 1992; Page & Applegate 1992); (2) reheating due to frictional coupling of the crust and a separately rotating superfluid component (Shibazaki & Lamb 1989); (3) presence of exotic matter in the NS core (Shibazaki & Lamb 1989; Page

& Baron 1990); (4) effects of superfluidity in the NS crust (Nomoto & Tsuruta 1987; Shibazaki & Lamb 1989); and (5) the possibility of crust bremsstrahlung suppression due to band structure effects (Pethick & Thorsson 1994). Observations of cooling NSs have been reviewed recently by Ögelman (1994) who finds that the most convincing cases for cooling do not require the extended direct Urca cooling, nor do they suggest the presence of exotic material in the core which would lead to rapid cooling.

To investigate such scenarios for the emission from PSR 0355+54, we have considered emission from the entire surface of a NS with $R = 10$ km. This scenario is consistent with the lack of observed pulsations, although the limit derived for the pulsed fraction is not particularly constraining in this regard. To derive an effective surface temperature which, given the characteristic age of the pulsar, may be compared with cooling models, we assume a column density $N_H = 2 \times 10^{21}$ cm^{-2} derived from 21 cm absorption measurements. For a distance of 2.1 kpc (Taylor et al. 1993), a blackbody temperature $kT = 82 \pm 4$ eV $[T = 9.5(\pm 0.5) \times 10^5$ K] is required to produce the observed PSPC count rate. This yields a luminosity $L_x(0.1\text{–}2.4 \text{ keV}) = 5.7 \times 10^{32}$ ergs s^{-1}. The corresponding surface temperature, when corrected for gravitational redshift assuming a 1.4 $M_\odot$ NS of radius 10 km (Helfand, Channan, & Novick 1980) is $kT = 108 \pm 5$ eV $[T = 1.25(\pm 0.07) \times 10^6$ K].

A thermal spectrum emitted from the NS surface will undergo modification in the presence of an atmosphere (Miller 1992; Shibanov et al. 1992) which may result in an enhancement of the Wien tail of the blackbody spectrum (at the expense of the Rayleigh-Jeans region). The effective temperature derived from the modified spectrum may vary considerably from that of a pure blackbody; Ögelman & Finley (1993) find nearly a factor of 2 difference in the effective temperature for a Shibanov et al. (1992) model when comparing it to an unmodified blackbody using PSR 1055−52 data obtained with the *ROSAT* PSPC. Similar calculations by Miller (1992) predict a somewhat smaller effect for *ROSAT* HRI observations. The effect is dependent upon both the magnetic field strength and the NS surface temperature and composition. The derived effective temperatue further depends upon the spectral response of the detectors; if the effective area peaks where the spectrum is relatively unmodified, the derived temperature will be close to the actual surface temperature. Attempts at modeling the atmosphere effects are beyond the scope of this paper, and the number of photons collected, but inspection of previous results suggests that presence of an atmosphere would not change the derived temperature for PSR 0355+54 by as much as a factor of 2.

The derived temperature falls above current cooling models (Fig. 2). The data thus fail to constrain the models even though the derived temperature must be considered an upper limit since contribution from another emission component cannot be ruled out by the data; indeed, as we discuss below, the bulk of the emission appears to be derived from the pulsar spin-down.

Since the blackbody normalization is set by the pulsar radius and distance, and we have also specified the value of N_H, the temperature is the only free parameter in the above analysis; the uncertainty in temperature reflects the uncertainty in the count rate. In reality, we have enough spectral information to confront this scenario more critically by considering the derived hardness ratios H_1 and H_2. Keeping the blackbody normalization fixed, we have considered a range of

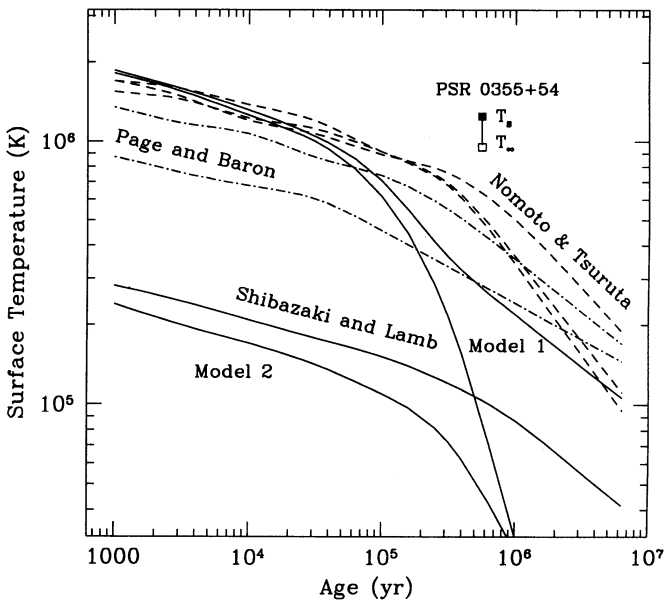

FIG. 2.—Models for cooling of neutron star interior. References to models are given in text. Shibazaki & Lamb model 1 is for standard cooling with no reheating (*lower*) and reheating due to frictional coupling between crust and superfluid core; model 2 includes effects of pion condensates in core. Page & Baron models are for no superfluid, no exotic matter (*upper*) and superfluid with kaon condensates (*lower*). Nomoto & Tsuruta models contain no exotic core matter, and: superfluid (*lower*), and no superfluid (*upper*) for soft equation of state; no superfluid (*middle*) with stiff equation of state. Effective temperature at surface T_s and at infinity T_∞ for PSR 0355+54 is higher than all models, suggesting a spin-down origin for at least some fraction of the emission.

N_H values and calculated the temperatures required to produce the observed count rate. We then generated models of these spectra, folded them through the PSPC spectral response, and calculated the associated hardness ratios. We find that blackbody emission from the entire surface, for any reasonable N_H values, cannot reproduce the observed hardness ratios (Fig. 3); the observed spectrum is harder than can be accommodated with emission from the entire surface. We note, however, that thermal emission from a hot polar cap is not ruled out by these measurements (see § 5). We also find that accretion from the ISM cannot account for the observed luminosity (see § 5). We conclude that the emission is primarily associated with either the pulsar magnetosphere or a compact synchrotron nebula; in either case, it is derived primarily from the pulsar's spin-down power. This indicates that the above temperature must be considered a strong upper limit; more sensitive observations are needed to define better the spectrum in order to assess the contribution of cooling to the total X-ray flux.

4.2. *Power-Law Emission*

X-rays associated with energy derived from the pulsar magnetosphere can be produced in several ways. A relativistic electron wind may be confined by the ambient circumstellar magnetic field, resulting in a synchrotron nebula such as those associated with the Crab and Vela pulsars. Alternatively, direct magnetospheric X-rays can be produced in polar or outer gap regions where charge depletion allows strong $\boldsymbol{E}$ fields to develop along the NS magnetic field lines.

In outer gap models, high-energy radiation is produced through a bootstrap mechanism whereby energetic primary electrons generate γ-rays which, in turn, result in a pair-

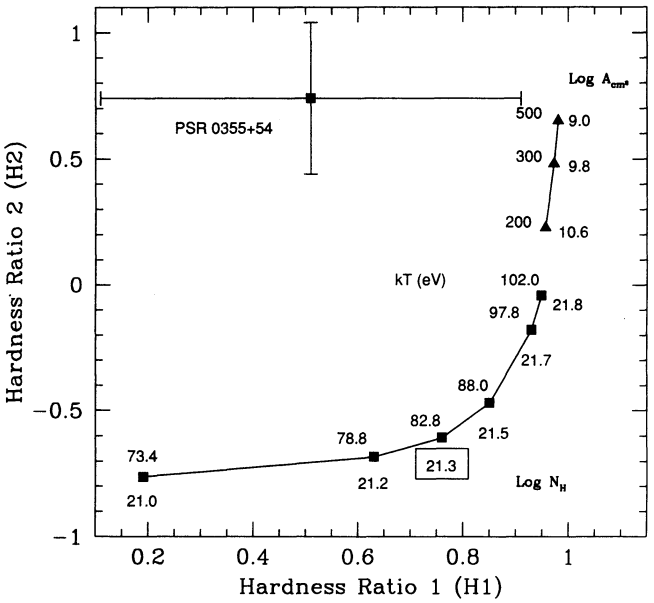

FIG. 3.—Hardness ratios derived for PSPC data for PSR 0355+54. Connected points show hardness ratios derived for models of blackbody emission from surface of a neutron star with 10 km radius (*squares*), and for blackbody emission from a hot polar cap (*triangle*). Upper numbers correspond to temperature (kT in eV), and lower numbers correspond to log N_H values (for squares—21 cm value is indicated by box, and plot extends to 3 times this value to cover any reasonable values of N_H) or areas of emitting regions (*triangles*) required to produce observed number of source counts.

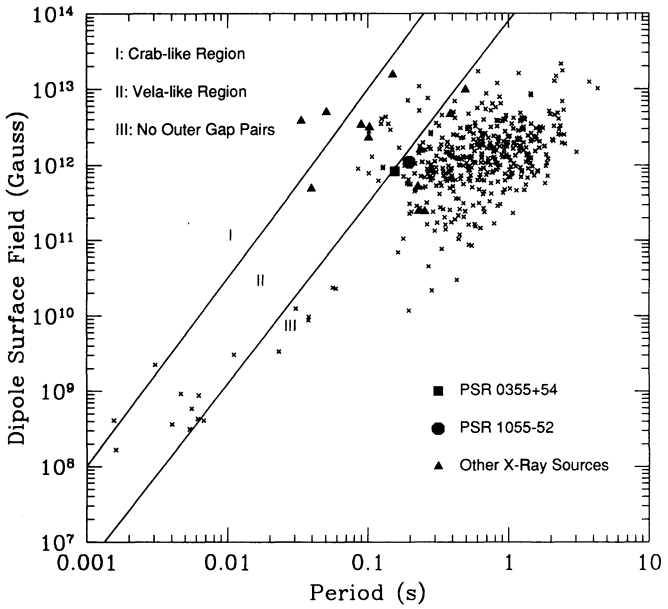

FIG. 4.—Magnetic field vs. rotation period for all pulsars. Death lines for Crab-like and Vela-like outer gap emission are indicated (after Cheng & Ruderman 1993). Known X-ray emitters are indicated. PSR 0355+54, like PSR 1055−52, lies at death line for Vela-like emission. In this region γ-rays dominate the outer gap emission, making PSR 0355+54 a good candidate for γ-ray study.

production cascade; the secondary electrons boost ambient photons to high energies through inverse Compton scattering. Heating of the polar cap from backflow of relativisitic electrons may produce soft X-ray emission. The magnetosphere can be classified as "Crab-like" or "Vela-like" based upon whether curvature radiation or inverse Compton scattering is the dominant initial mechanism (Cheng, Ho, & Ruderman 1986a, b). A "death line" for the outer gap mechanism can also be derived (Chen & Ruderman 1993) based upon the values of P and B (Fig. 4). The γ-ray production efficiency $L_\gamma/\dot{E}$ increases as pulsars approach this death line.

In polar cap models (e.g., Daugherty & Harding 1982) curvature radiation in polar cap gap regions is responsible for the γ-ray production. Bombardment of the polar caps results in heating and soft X-ray production. This scenario has been proposed to explain X-ray and γ-ray results from Geminga (Harding, Ozernoy, & Usov 1994), and may explain the relatively hard emission from PSR 0355+54.

PSR 0355+54 falls just below the death line for outer-gap emission, as do several isolated X-ray emitting pulsars, though this line is actually somewhat dependent upon the inclination between the $\boldsymbol{B}$ field and the rotation axis. PSR 1055−52 also falls just below the death line; X-ray and γ-ray emission suggest this source may actually operate under Vela-like acceleration conditions. This suggests the strong possibility that PSR 0355+54, like PSR 1055−52, could be an observable γ-ray source.

To investigate the characteristics of any power-law emission, we have assumed a Crab-like spectrum (photon index $\alpha = 2$) and $N_H = 2 \times 10^{21}$ cm^{-2}, as before. For such a spectrum, we find an X-ray luminosity $L_x(0.1\text{–}2.4\ \text{keV}) = 1.0 \times 10^{32}$ ergs s^{-1}. This is consistent with observed luminosities for other pulsars (Fig. 5). In particular, it is very similar to that which we derive for the power-law component from PSR 1055−52; using the PSR 1055−52 spectral index of 1.5 (see Table 3) reduces the PSR 0355+54 luminosity by a factor of 2. The PSR 0355+54 results are in good agreement with other spin-down correlations, which further supports the interpretation of nonthermal emission.

5. DISCUSSION

The prospect of accretion from the ISM as the source of the X-ray luminosity has been discussed by Treves & Colpi (1991).

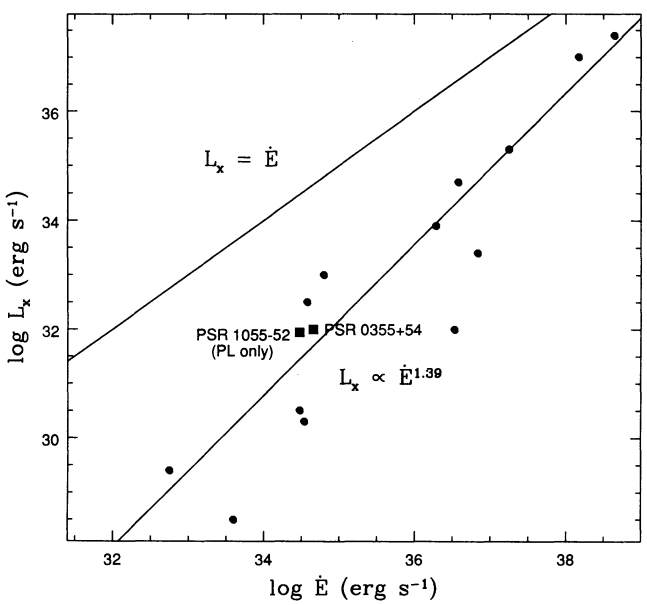

FIG. 5.—X-ray luminosity vs. spin-down power for known X-ray emitting isolated pulsars (after Seward & Wang 1988); luminosity values are from Ögelman (1994). PSR 0355+54 luminosity agrees well with other pulsar values, in particular that for the power-law component of PSR 1055−52, suggesting emission is derived from the pulsar spin-down.

The measured proper motion for PSR 0355+54 is ~ 8 mas yr^{-1} (Lyne et al. 1982). For a distance of 2.1 kpc, this provides a velocity lower limit $v \geq 30$ km s^{-1}. For spherically symmetric accretion, the accretion rate for a star moving through the ISM is (Bondi & Hoyle 1944; see Helfand et al. 1980)

$$\dot{M} = 3.73 \times 10^8 \left(\frac{M}{M_\odot}\right)^2 n_{\rm H} v_{100}^{-3} , \quad (4)$$

where $n_{\rm H}$ is number density of the ambient medium and v_{100} is NS velocity in units of 100 km s^{-1}. Assuming a mass conversion efficiency $\dot{E} = 0.1\dot{M}c^2$, typical of values derived for accretion onto a NS in binary systems, this yields $L_x = 2 \times 10^{30}$ ergs s^{-1} for $n_{\rm H} = 1$ cm^{-3}, which is more than twice the average value assuming the values of N_H and D used above; an increase of $n_{\rm H}$ by two orders of magnitude would be required to yield the observed luminosity, which seems quite unreasonable.

We have shown that the hardness ratios derived from the PSR 0355+54 data are not consistent with thermal emission from the entire NS surface, and have thus concluded that the bulk of the emission cannot be attributed to cooling of the NS interior. A thermal spectrum at higher temperature, with a corresponding reduction in the size of the emitting region, is a distinct possibility, however. Such a scenario is expected in both polar and outer gap models due to heating of the polar caps by streams of energetic particles, and such a model has been proposed to describe X-ray data from PSR 1929+10 (Yancopoulos, Hamilton, & Helfand 1994). For an aligned dipole field, the size of the polar cap is defined by the last closed field line:

$$r_{\rm cap} = \sqrt{\left(\frac{2\pi R^3}{cP}\right)} . \quad (5)$$

We may thus use the PSR 0355+54 period to calculate an emitting area for the polar cap in an aligned rotator: $A = 4.3 \times 10^9$ cm^2. Along with the distance, this defines the normalization for a model of blackbody emission from the polar caps. In order to reproduce the observed count rate, again assuming $N_H = 2 \times 10^{21}$ cm^{-2}, the cap temperature (corrected for redshift) must be $kT = 301.6$ eV ($T = 3.5 \times 10^6$ K). A model spectrum with these parameters again fails to reproduce the observed hardness ratios, although it provides a better representation than can be accomplished with models for emission from the entire surface; it may indeed be possible to reproduce the results with proper combinations of A, T, and N_H, but the data are not sufficient to permit such independent determinations. In Figure 3 we plot hardness ratios derived for blackbody models with N_H fixed as above, and with temperature and emitting area varying so as to produce the observed count rate for PSR 0355+54. We note that the temperature derived above is very similar to that found for apparent polar cap emission from PSR 1929+10 (Yancopoulos et al. 1994).

For a nearly orthogonal dipole, the X-ray luminosity resulting from bombardment of the polar caps is (Arons 1981a; Harding et al. 1994)

$$L_x \approx 4 \times 10^{26} \mu_{30} P^{-27/8} \text{ ergs s}^{-1} , \quad (6)$$

where μ_{30} is the pulsar magnetic dipole moment in units of 10^{30} G cm^3. For PRS 0355+54, this predicts a luminosity $L_x \approx 10^{29}$ ergs s^{-1} which is considerably smaller than the observed luminosity. Additional heating associated with positron trapping (and subsequent acceleration toward the poles) in the weak-field outer regions of the magnetosphere may increase the luminosity to $\sim 10^{31}$ ergs s^{-1} (Arons 1981b), still too small to agree with the observations; further, this mechanism may only be applicable to slow pulsars with relatively small fields. It would appear that, if polar cap emission is indeed responsible for the X-ray emission, the associated particle acceleration does not occur (at least uniquely) in the polar regions.

As shown in Figure 5, the luminosity derived for PSR 0355+54 corresponds well to that of other isolated pulsars based upon the available spin-down power. The solid lines indicated in the figure correspond to $L_x = \dot{E}$ and

$$L_x = 2.5 \times 10^{-17} \dot{E}^{1.39} , \quad (7)$$

an empirical relationship derived by Seward & Wang (1988) based upon *Einstein* results; Ögelman (1994) finds a similar result based upon more recent *ROSAT* pulsar detections. In the figure, we have indicated the luminosity of the power-law component only for PSR 1055−52 (see Table 3). This value is in excellent agreement with the derived luminosity for PSR 0355+54, as one might expect given the similarity in parameters, and gives further indication that the observed emission is derived from the spin-down.

In PSR 1055−52, the power-law component appears to extend from the X-ray to the γ-ray range; the spectral values given in Table 3 predict a γ-ray flux $F(E > 100$ MeV$) = 4.1 \times 10^{-7}$ photons cm^{-2} s^{-1}, in reasonable agreement with the observed value of $2.7(\pm 0.5) \times 10^{-7}$ photons cm^{-2} s^{-1}. This suggests an association between the emission mechanisms which might be expected to hold for PSR 0355+54. Assuming the same power-law index leads to a predicted γ-ray flux $F(E > 100$ MeV$) = 1.9 \times 10^{-7}$ photons cm^{-2} s^{-1}. Clearly there are mitigating factors, such as magnetic field orientation and geometry, which make such an estimate quite uncertain. Current limits on emission from PSR 0355+54 derived from EGRET data are (Thompson et al. 1994) $F(E > 100$ MeV$) = 2.8 \times 10^{-7}$ photons cm^{-2} s^{-1} and $F(E > 1$ GeV$) = 2.4 \times 10^{-8}$ photons cm^{-2} s^{-1}. Based upon the X-ray luminosity and known γ-ray behavior of PSR 1055−52, it appears extremely worthwhile to pursue further γ-ray studies of PSR 0355+54.

The author would like to thank H. Ögelman, M. C. Miller, and A. Harding who all provided helpful insight in interpreting the results. Thanks also to D. Helfand whose comments and suggestions, as referee, helped clarify and strengthen many portions of the text. This work was supported by the National Aeronautics and Space Administration through grant NAG5-2329, and contract NAS8-39073.

REFERENCES

Alpar, M. A., Pines, D., & Cheng, K. S. 1988, Nature, 348, 707
Arons, J. 1981a, ApJ, 248, 1099
———. 1981b, in IAU Symp. 95, Pulsars, ed. W. Sieber & R. Wielebinski (Dordrecht: Reidel), 69
Bondi, H., & Hoyle, F. 1944, MNRAS, 104, 273
Brinkmann, W., & Ögelman, H. 1987, A&A, 182, 71
Buccheri, R., et al. 1983, A&A, 128, 245
Chen, K., & Ruderman, M. 1993, ApJ, 402, 264
Cheng, A. F. 1983, ApJ, 275, 790
Cheng, A. F., & Helfand, D. J. 1983, ApJ, 217, 271
Cheng, K. S., Ho, C., & Ruderman, M. 1986a, ApJ, 300, 500
———. 1986b, ApJ, 300, 522
Daugherty, J. K., & Harding, A. K. 1982, ApJ, 252, 337
Fierro, J. M., et al. 1993, ApJ, 413, L27
Finley, J. P. 1994, in Proc. *ROSAT* Science Symposium, in press
Gómez-Gonzàlez, J., & Guélin, M. 1974, A&A, 32, 441
Harding, A. K., Ozernoy, L. M., & Usov, V. V. 1994, MNRAS, in press
Helfand, D. J. 1983, in IAU Symp. 101, Supernova Remnants and Their X-Ray Emission, ed. J. Danzinger & P. Gorenstein (Dordrecht: Reidel), 471
Helfand, D. J., Channan, G. A., & Novick, R. 1980, Nature, 283, 337
Lattimer, J. M., et al. 1991, Phys. Rev. Lett., 66, 2701
Lyne, A. G. 1987, Nature 326, 569
Lyne, A. G., Anderson, B., & Salter, M. J. 1982, MNRAS, 201, 503
McCulloch, P. M., et al. 1978, MNRAS, 183, 645
Miller, M. C. 1992, MNRAS, 255, 129
Morris, D. A., et al. 1981, A&AS, 46, 421
Nomoto, K., & Tsuruta, S. 1986, ApJ, 305, L19
Ögelman, H. 1994, in Proc. 1993 September NATO ASI on Lives of Neutron Stars, Kemer, Turkey, in press
Ögelman, H., & Finley, J. P. 1993, ApJ, 413, L31
Page, D., & Applegate, J. H. 1992, ApJ, 394, L17
Page, D., & Baron, E., 1990, ApJ, 354, L17
Pethick, C. J., & Thorsson, V. 1994, Phys. Rev. Lett., submitted
Pfeffermann, E., et al. 1986, Proc. SPIE, 733, 519
Seward, F. D., & Wang, Z-R. 1988, ApJ, 332, 199
Shibazaki, N., & Lamb, F. K. 1989, ApJ, 346, 808
Shibanov, Y. A., et al. 1992, A&A, 266, 313
Taylor, J. H., Manchester, R. N., & Lyne, A. G. 1993, ApJS, 88, 529
Thompson, D. J. 1994, ApJ, submitted
Treves, A., & Colpi, M. 1991, A&A, 241, 107
van der Klis, M. 1989, in Timing Neutron Stars, in Proc. NATO ASI on Timing Neutron Stars, ed. H. Ögelman & E. P. J. van den Heuvel (Dordrecht: Kluwer), 27
Wang, Q. D., Li, Z-Y., & Begelman, M. C. 1993, Nature, 364, 127
Yancopoulos, S., Hamilton, T. T., & Helfand, D. J. 1994, ApJ, submitted